A Total Lightning Trending Algorithm to Identify Severe Thunderstorms

PATRICK N. GATLIN

Earth Systems Science Center, University of Alabama in Huntsville, Huntsville, Alabama

STEVEN J. GOODMAN

NOAA/NESDIS, GOES-R System Program Office, NASA Goddard Space Flight Center, Greenbelt, Maryland

(Manuscript received 23 January 2009, in final form 14 July 2009)

ABSTRACT

An algorithm that provides an early indication of impending severe weather from observed trends in thunderstorm total lightning flash rates has been developed. The algorithm framework has been tested on 20 thunderstorms, including 1 nonsevere storm, which occurred over the course of six separate days during the spring months of 2002 and 2003. The identified surges in lightning rate (or jumps) are compared against 110 documented severe weather events produced by these thunderstorms as they moved across portions of northern Alabama and southern Tennessee. Lightning jumps precede 90% of these severe weather events, with as much as a 27-min advance notification of impending severe weather on the ground. However, 37% of lightning jumps are not followed by severe weather reports. Various configurations of the algorithm are tested, and the highest critical success index attained is 0.49. Results suggest that this lightning jump algorithm may be a useful operational diagnostic tool for severe thunderstorm potential.

1. Introduction

The purpose of this study is to examine the utility of using trends in total lightning activity to help diagnose the severe weather potential of a thunderstorm. An algorithm derived from total lightning data measurements (both cloud and ground flashes) has been developed to help gauge thunderstorm intensity. This algorithm attempts to predict severe weather without the use of any radar observables. The proposed total lightning algorithm is based upon the observations of rapid increases of total lightning activity preceding severe and tornadic thunderstorms (Williams et al. 1999; Goodman et al. 2005). These rapid increases in the total flash rate found to precede severe weather at the ground have been termed ''lightning jumps'' by Williams et al. (1999).

Lightning jumps are characterized by a rapid increase in total lightning activity followed by a relative maximum and ending with a slow decline in lightning activity. This trend in lightning activity is believed to be the electrical response to updraft behavior during thunderstorm evolution, which is supported by both theoretical and observational studies relating updraft evolution and total lightning flash rate (e.g., Williams et al. 1989; Baker et al. 1995, 1999; Deierling 2006). During rapid growth of the updraft within a thundercloud, more frequent collisions between ice crystals and rapidly growing graupel in the presence of enhanced supercooled liquid water produce an increase of lightning flash rate. Lightning activity peaks around the same time as the updraft speed reaches maximum growth (speed and volume) and then decreases as the updraft weakens. This correlation between updraft and lightning activity is exemplified in the 20 July 1986 microburst-producing thunderstorm observed by Goodman et al. 1988 (Fig. 1). Figure 1 shows the intracloud lightning activity peaks after the maximum vertical velocity, during the highest altitude of the 30-dBZ reflectivity echo and prior to the maximum differential velocity and microburst winds impacting the ground.

Although there have been several studies that discuss lightning jumps (e.g., Williams et al. 1999; Goodman et al. 2005; Steiger et al. 2007), there has yet to be any objective method in the literature defining a lightning jump. Furthermore, the regular use of total lightning data in operational meteorology is going to increase

Corresponding author address: Patrick Gatlin, ESSC/UAH, 320 Sparkman Dr., Huntsville, AL 35805.
E-mail: gatlin@nsstc.uah.edu

DOI: 10.1175/2009JTECHA1286.1

© 2010 American Meteorological Society

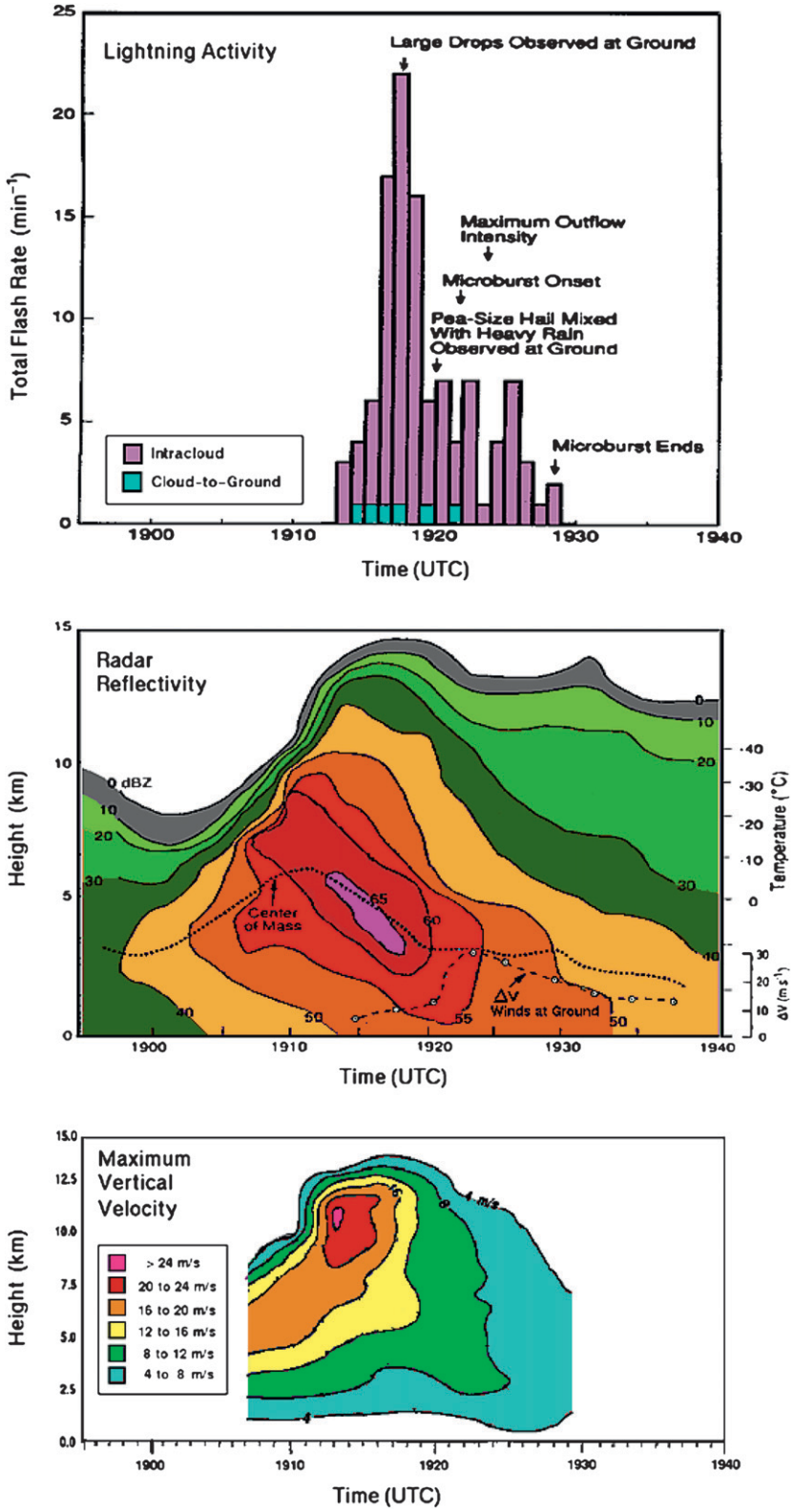

FIG. 1. Lightning and precipitation history of a microburst-producing thunderstorm observed on 20 Jul 1986, during the Cooperative Huntsville Meteorological Experiment (adapted from Goodman et al. 1988; Kingsmill and Wakimoto 1991).

when the Geostationary Operational Environmental Satellite (GOES-R) Geostationary Lightning Mapper (GLM) is launched (Goodman et al. 2006). National Weather Service (NWS) forecast offices having access to regional, ground-based total lightning very-high-frequency (VHF) mapping systems can only subjectively analyze trends in lightning activity, which just adds additional burden on the forecaster during the warning decision-making process. The only algorithms used operationally in NWS forecast offices to predict severe weather onset are radar based (e.g., Mitchell et al. 1998; Stumpf et al. 1998; Witt et al. 1998a). Total lightning data has been shown to be useful in the warning decision-making process (e.g., Darden et al. 2006; Demetriades et al. 2008), but there exists no quantitative algorithm or uniform methodology in NWS operations that utilizes the total lightning data to predict severe weather onset. Thus, there is a need for an algorithm that can exploit the trends in total lightning activity often found to precede severe weather. The algorithm presented in this study has been developed to not only quantify the lightning jump but also provide operational meteorologists with an initial total lightning data tool that can be used to monitor thunderstorm intensity and aid in the warning decision-making process.

The lightning jump algorithm developed in this study is tested on a dataset containing 20 thunderstorms observed with the North Alabama Lightning Mapping Array (LMA; Goodman et al. 2005). Results are compared with the 110 severe weather events distributed unevenly among 19 of these thunderstorms (no severe weather was observed with one storm). The following section explains how lightning flashes are detected and defined and how the lightning jump is identified. Section 3 provides observational evidence of the lightning jump and physical processes that take place resulting in the rapid increase in lightning activity prior to severe weather. An overview of several of the thunderstorm cases as well as application of the lightning jump algorithm to each is presented in section 4. Section 5 discusses the algorithm performance with respect to the severe weather events and how these findings compare to previous studies.

2. Methodology

a. North Alabama Lightning Mapping Array

The North Alabama LMA consists of 10 stations located across northern Alabama, with a central processing site at the National Space Science and Technology Center (NSSTC) in Huntsville, Alabama (Fig. 2). Each station uses GPS technology to measure the time of arrival of VHF radio impulses in the 76–82-MHz range and records only the most powerful impulse occurring within an 80-μs window (Rison et al. 1999). The arrival times recorded at each of the LMA stations are compared in order to locate, in four dimensions (spatially and temporally), impulsive VHF radiation sources associated with the lightning channel (Proctor 1971; Rison et al. 1999). The data used in this study are confined to within 160 km of the NSSTC (Fig. 2) to minimize the error associated with the calculation of individual radiation source locations (Koshak et al. 2004; McCaul et al. 2009).

b. Source clustering (flash) algorithm

The complete (i.e., postprocessed) LMA dataset was used to reconstruct the lightning channels. These VHF sources were put through a flash clustering algorithm, which applies both temporal and spatial proximity tests to the sources and either assigns each source to a flash or classifies it as system noise (McCaul et al. 2005, 2009). A source is assigned to a flash if it occurs within 0.3 s of a prior source and if the source satisfies the spatial proximity requirement. The maximum spatial separation allowed between successive candidate sources is governed by their distance away from the center of the network, which is addressed by LMA location uncertainty (Koshak et al. 2004). Since the uncertainty in the distance of a source from the center of the LMA network and its altitude increases quadratically with range and the LMA detection efficiency decreases with range, it has been assumed that the maximum range difference between consecutive sources, which belong to the same flash, increases with the square of the distance from the network. Thus, two sources that are candidates for the same flash may be separated by no more than 10 km in range at a distance of 100 km. The azimuthal uncertainty in source location is bounded by 0.05 rad (McCaul et al. 2009), and thus at 100 km from the LMA center, a candidate source must not be more than 5 km away from the previous candidate source. Unlike other flash clustering algorithms (e.g., Williams et al. 1999; Thomas et al. 2003), the North Alabama algorithm does not place any upper bound on flash duration, yet results from the North Alabama LMA flash algorithm agree well (within ~5%) with output from the flash algorithm designed by Thomas et al. (2003).

This version of the North Alabama flash algorithm (McCaul et al. 2005) also does not place any lower limit on the number of VHF sources required to reconstruct a lightning flash. However, the algorithm is able to classify some lone sources as noise and others as single-source flashes (i.e., "singletons") based upon their signal strength. Although singleton events are not expected to greatly affect the flash rate trend (Wiens et al. 2005), the

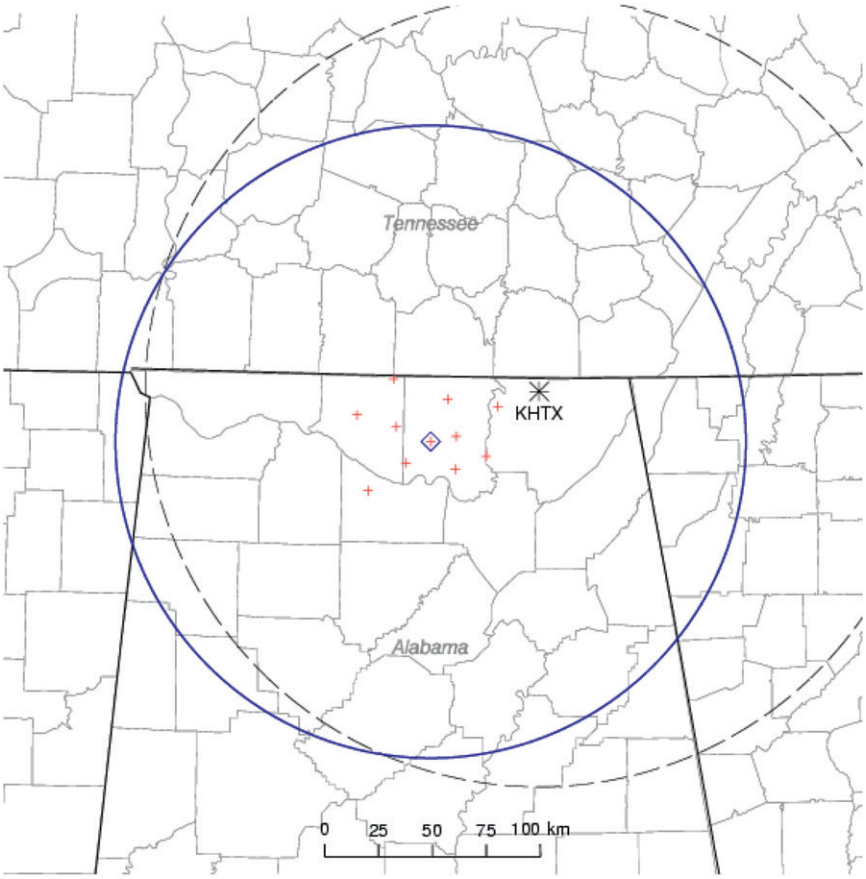

FIG. 2. Map of the study domain centered on northern Alabama. LMA antenna locations (crosses) and range rings for the LMA (solid) and KHTX (dashed) are also shown. The center of the LMA is at the NSSTC (diamond).

flash definition was tested using a 0, 5, 10, and 30 minimum VHF source constraint in the calculation of total flash rate.

The number of flashes produced by a storm was determined by confining the flash data to within either a 10- or 15-km radius, depending on storm size, of the greatest electrical activity within the thunderstorm, which was determined by tracking the VHF source density maximum. The VHF source density field, calculated by counting the number of VHF sources detected by the LMA in a 2 km $\times$ 2 km vertically integrated grid box, was used to locate regions of the storm with the greatest electrical activity. The 10–15-km constraint was chosen in order to encompass the storm of interest while minimizing the inclusion of flashes produced by neighboring storms. Others have used similar methods of assigning flashes to a storm (e.g., Williams et al. 1999; Goodman et al. 2005; McCaul et al. 2005). The simple constraint employed here would make flash assignment quick and easy for operational implementation. For example, flashes could be assigned to a storm based upon their proximity (perhaps via inverse distance weighting with a neighborhood size of 10–15-km radius) to the storm of interest. Occasionally, the 10–15-km radial constraint may not encompass all lightning flashes produced, especially by large thunderstorms (i.e., those exceeding 20 km in extent), and thus this method can lead to an underestimation of the true total flash rate. However, the vast majority of lightning flashes produced by the thunderstorms in this study are captured within the assigned radius of constraint.

Cloud-to-ground (CG) flashes were detected using the National Lightning Detection Network (NLDN; Cummins et al. 2006). To remove intracloud flash detections falsely reported as CG flashes, all positive CG (+CG) flashes with amplitudes less than 10 kA were removed, in an approximate way to Cummins et al. (1998, 2006), from the NLDN dataset included in this study.

c. *Lightning jump algorithm*

The lightning jump algorithm tracks trends in the total flash rate and objectively identifies lightning jumps. It uses only the total flash rate derived from the VHF

source observations of the LMA. The jump algorithm was tested on both the 1- and 2-min total flash rates. The 1-min total flash rate is the number of flashes occurring within a 1-min time period, whereas the 2-min total flash rate is the total flash rate averaged over a 2-min period of time. To determine the trend and quantify the lightning jump, the time rate of change of the total flash rate f' is calculated as

$$f' = \frac{d}{dt} f \cong \frac{f(t + \Delta t) - f(t)}{\Delta t},$$

where f is the total flash rate and its derivative is estimated via finite difference. This algorithm treats the lightning jump as an anomaly relative to the average total flash rate. Thus, to identify this anomaly, the total flash rate f' must become significantly larger than average during a jump. Thus, the lightning jump threshold f'_{thres} is defined as

$$f'_{\text{thres}} \equiv \overline{f'} + 2\sigma(f'),$$

where $\sigma(f')$ is the standard deviation of f' and $\overline{f'}$ is its moving average. This standard deviation and moving average were calculated from either the prior 6–10-min history of the 1-min-derived f' or the 12–20-min history of 2-min-derived f', depending upon algorithm configuration. Since the lightning jump is an increase in total flash rate that must exceed two standard deviations of the moving average, the jump threshold will always be positive. The jump threshold was also modified, as explained further in the appendix, to be less sensitive to minor fluctuations in the lightning activity that may occur over short time intervals and lead to an inflated number of false alarms. To determine the averaging and thresholding techniques that would maximize the severe weather detections while trying to minimize the number of false detections, the lightning jump algorithm was configured with five different configurable parameters as follows:

1) sampling rate (i.e., 1- or 2-min f);
2) calculation of moving average of f, f', and f'_{thres} (see the appendix; standard, weighted, or a combination of both = 8 elements);
3) time interval used for moving average calculation of f, f', and f'_{thres} (0 min for standard mean and 2–6, 8- or 10-min samples for weighted mean depending upon sampling rate = 5^3 elements);
4) number of samples used to derive the standard deviation of f' (6 or 10 samples = 2 elements);
5) minimum number of sources used to define a flash (0, 5, 10, or 30 sources = 4 elements).

Since the lightning jump algorithm is dependent upon these five configurable parameters and their various elements, there are a total of 10 000 possible algorithm configurations ($8 \times 5^3 \times 2 \times 4 + 8 \times 5^3 \times 2 = 10\,000$). Each configuration, which consists of a unique combination of the elements belonging to the five parameters, was tested to determine which yields the best results. The best configuration is the one that results in the highest probability of detection (POD) and lowest false alarm rate [(FAR); highest critical success index (CSI)]. Singletons were not removed from the 1-min total flash rate, and thus no sensitivity tests are performed on flash definition when using a 1-min total flash rate.

Figure 3 illustrates how a lightning jump is classified for the purposes of this study. A lightning jump occurs when f' exceeds the jump threshold (squares in Fig. 3), and the peak of the lightning jump is the highest flash rate attained (i.e., local maximum in total flash rate after the jump occurs; diamonds in Fig. 3). To factor out small fluctuations in the flash rate during a lightning jump, f' must decrease below $\overline{f'}$ to signify the end of the lightning jump.

To determine the extent to which the conceptual lightning jump framework can be solely used (absent the use of any radar observables) as a predictor for severe weather onset, the POD, FAR, and CSI are used to conduct a categorical verification (Wilks 1995) and are calculated as follows:

$$\text{POD} \equiv \frac{\text{hits}}{\text{hits} + \text{misses}},$$

$$\text{FAR} \equiv \frac{\text{false alarms}}{\text{hits} + \text{false alarms}},$$

$$\text{CSI} \equiv \frac{\text{hits}}{\text{hits} + \text{false alarms} + \text{misses}}.$$

A *hit* occurs when a lightning jump (notated by t_0 in Fig. 3) occurs prior to severe weather and the jump peak (noted by t_1 in Fig. 3) precedes a documented severe weather occurrence (noted by t_2 in Fig. 3) by no more than 30 min (i.e., $t_0 < t_2$ and $t_2 - t_1 \leq 30$ min). A *miss* occurs when a severe weather event is not preceded within 30 min by a lightning jump. A *false alarm* is a lightning jump that is not followed within 30 min by a severe weather event (see Fig. 3). This 30-min constraint is based on the findings of Williams et al. (1999) and Goodman et al. (2005) that show lightning jumps mostly occurring 5–25 min prior to severe weather events. The time constraint should allow for sufficient advance warning (Simmons and Sutter 2008).

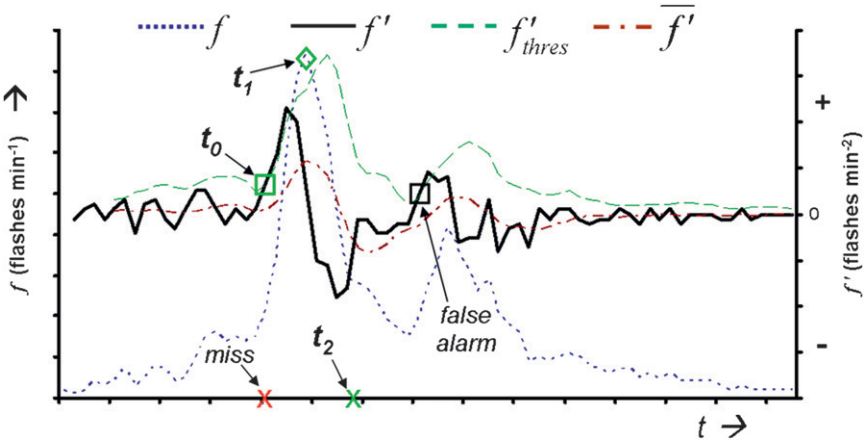

FIG. 3. Example of the lightning jump threshold (dashed line) applied to the change in flash rate (solid line) of a thunderstorm with severe weather events (crosses) on the abscissa. Lightning jumps occur when f' exceeds f'_{thres} (squares). A jump is classified as a hit at time t_0 (green square) when it precedes a severe weather event at time t_2 (green cross). The peak total flash rate attained during a jump is indicated at time t_1 (green diamond). The severe weather event annotated as a "miss" had no preceding lightning jump. Total flash rate (dotted line) and the moving average of the change in flash rate (dash–dot line) are also plotted.

A severe weather event is defined as the occurrence of at least one of the following: hail with diameter exceeding 1.9 cm (0.75 in.), straight-line winds exceeding 26 m s^{-1} (50 kt), or a tornado. Four funnel cloud reports are also grouped with the severe weather events in this study. Severe weather locations and times are taken from the National Climatic Data Center *Storm Data* database. These severe weather events were assigned to each thunderstorm by examining their proximity and timing relative to the storm. To avoid inflating the total number of hits, multiple severe weather events that occurred within 6 min of each other were considered as one event when determining POD, FAR, and CSI. This also allows for a possible timing discrepancy between the actual and reported time of severe weather occurrence recorded in *Storm Data* (refer to Witt et al. 1998b). However, through collaboration with the local NWS weather forecast office in Huntsville, Alabama (e.g., Darden et al. 2006), the authors have checked each storm report against the radar data to ensure the reported timing and location are as accurate as possible.

d. Doppler radar–derived quantities

Radar data were collected with the NWS Weather Surveillance Radar-1988 Doppler (WSR-88D) at Hytop, Alabama (KHTX). Radar images in plan position indicator view and the corresponding vertical cross sections (Figs. 6, 8, and 10) were created with the Warning Decision Support System-integrated information (WDSS-II) software (Hondl 2002). The radar reflectivity was transformed from radar space (polar coordinates) into Cartesian coordinates using the REORDER software (Oye and Case 1995), in which the Cressman weighting scheme using a 1.0° × 1.0° × 1.0 km (azimuth × elevation × range) radius of influence was employed during the objective analysis to interpolate the radar data to a 1 km × 1 km × 0.5 km Cartesian grid. Using the gridded radar data, the location of each storm cell was determined by manually tracking the storm core (region of highest reflectivity). A 10–15-km radius from the storm core was then assigned to each cell in order to compute the maximum reflectivity at each vertical level and the vertically integrated liquid-water content (VIL; Greene and Clark 1972).

A Doppler radar analysis was conducted to explain the physical basis of the lightning jump in tornadic storms. The aliased Doppler velocities were corrected and storm rotation was determined by analyzing the radial velocity couplets, associated with either the mesocyclone or tornado vortex signature (whichever was present), for each elevation angle in the radar volume scan using the SOLO II software (Oye et al. 1995). The two opposing radial velocities equidistant from the radar, less than 10 km apart and yielding the largest cyclonic shear are determined and used to calculate the radial shear δ_r:

$$\delta_r = \frac{V_{\text{inbound}} - V_{\text{outbound}}}{\Delta r},$$

where Δr is the distance between the inbound V_{inbound} and outbound V_{outbound} radial velocities.

3. Physical reasoning for lightning jumps

Several studies (Williams et al. 1989; MacGorman et al. 1989; Williams et al. 1999; Goodman et al. 2005) indicate that the updraft is the main factor governing lightning flash rate. The updraft provides water—the fundamental ingredient needed for a cloud to build up enough electrical charge for lightning occurrence. Thus, an intense updraft supplies the cloud with ample water vapor, which leads to more condensate. The greater supply of condensate in turn leads to more ice particle collisions and thus greater charge separation and lightning (Williams 2001). It is also the updraft that governs storm severity. So it is necessary to examine the updraft evolution in relation to both lightning activity and storm strength (i.e., severe or not severe) in order to better explain the occurrence of lightning jumps. Thus, two cases with radar and lightning observations are presented below to further support the connection between the lightning jump and storm intensity.

a. Severe hailstorm case

Figure 4 shows the time–height evolution of radar reflectivity and electrical activity associated with a large-hail-producing thunderstorm that affected northern Alabama on 30 March 2002. The storm undergoes rapid vertical growth between 0310 and 0330 UTC, during which time the 50-dBZ reflectivity echo grows to 10 km and reflectivity in excess of 65 dBZ develops in the $-10°$ to $-20°$C region (Fig. 4a), indicating that precipitation-sized particles have grown and become more numerous. This suggests intense updraft growth through the mixed-phase region, which favors the growth of large hailstones. The updraft growth results in enhanced lightning activity as the total flash rate increases from 16 flashes per minute (hereafter flashes min^{-1}) at 0325 UTC to 84 flashes min^{-1} at 0335 UTC (Fig. 4b). The CG rate also shows a similar trend during this time but at a much lower magnitude; it only increases from 1 to 3 flashes min^{-1}. Minutes after the lightning jump, hail with 4.4-cm diameter was reported to be covering the ground.

b. Tornadic case

A similar trend is observed to occur in tornadic thunderstorms. Figure 5 illustrates the time–height evolution of radar reflectivity, Doppler radar–derived radial shear, and lightning activity of a tornadic minisupercell (Kennedy et al. 1993; Burgess et al. 1995) which occurred in northeastern Alabama on 19 March 2003. The storm undergoes rapid vertical growth from 1805 to 1825 UTC, indicated by the 50-dBZ reflectivity echo growth from 4- to 7-km altitude (Fig. 5a). Concurrently, the total flash rate rapidly increases from 3 to 38 flashes min^{-1} (Fig. 5c). Also, the radial shear increases at midlevels of the storm from 4 to 14 $\times$ 10^{-3} s^{-1} during this rapid increase in total flash rate, which is subjectively identified as a lightning jump (Fig. 5c). After 1825 UTC, the total flash rate gradually decreases as does the radial shear, decreasing to 8 $\times$ 10^{-3} s^{-1}, and the reflectivity echoes do not exhibit any additional vertical growth as strong as that before 1825 UTC. Although the shear decreases at midlevels there are indications of shear increasing at lower levels after 1830 UTC, suggesting descent of the mesocyclone.

The total flash rate exhibits a distinct resurgence between 1840 and 1848 UTC, indicative of the updraft strengthening once again (Fig. 5c). Although this updraft strengthening is not apparent in the VIL trends between 1840 and 1848 UTC, there is very weak vertical growth ($\sim$0.5 km) in the reflectivity echoes above 6 km during this time. Also during this time, the mesocyclonic shear deepens and extends from 1 to 6.5 km, indicating the contraction and stretching of the circulation. Within 5 min, an F1 tornado is observed under the mesocyclone location. A second F1 (F1-B) coexists with the first, but it is observed along the flanking line of the storm. The CG rate exhibits a similar trend to that of the total flash rate around 1820 UTC (Fig. 5b); however, the total flash rate increase is greater in magnitude. Both the total flash rate and CG rate increase once more prior to the tornado, but again the total flash rate increase at 1842 UTC is greater in magnitude. This total flash rate increase also occurs 8 min prior to the CG rate increase at 1850 UTC (when the first F1 tornado began).

c. Why lightning jumps occur prior to severe weather

As these severe storm cases have shown, there is rapid intensification of the updraft prior to severe weather being observed on the ground. This updraft surge quickly introduces more water vapor into the cloud and hence a higher concentration of ice particles, which collide with one another. The enhanced amount of condensate available and strong updraft speed lead to the growth of graupel-sized ice particles. The increased number of ice particle collisions, in turn, builds up electrical charge within the cloud and size sorting by the updraft separates the charge, thereby leading to increased intracloud lightning activity. Eventually the graupel grows large enough to fall from the updraft toward the ground. As a result, this creates excess drag on the updraft causing it to weaken and thereby resulting in fewer intracloud lightning flashes. The downdraft speed increases because of precipitation loading and evaporative cooling effects, accelerating hail and/or strong, possibly damaging, winds toward the surface. In tornadic storms, rapid

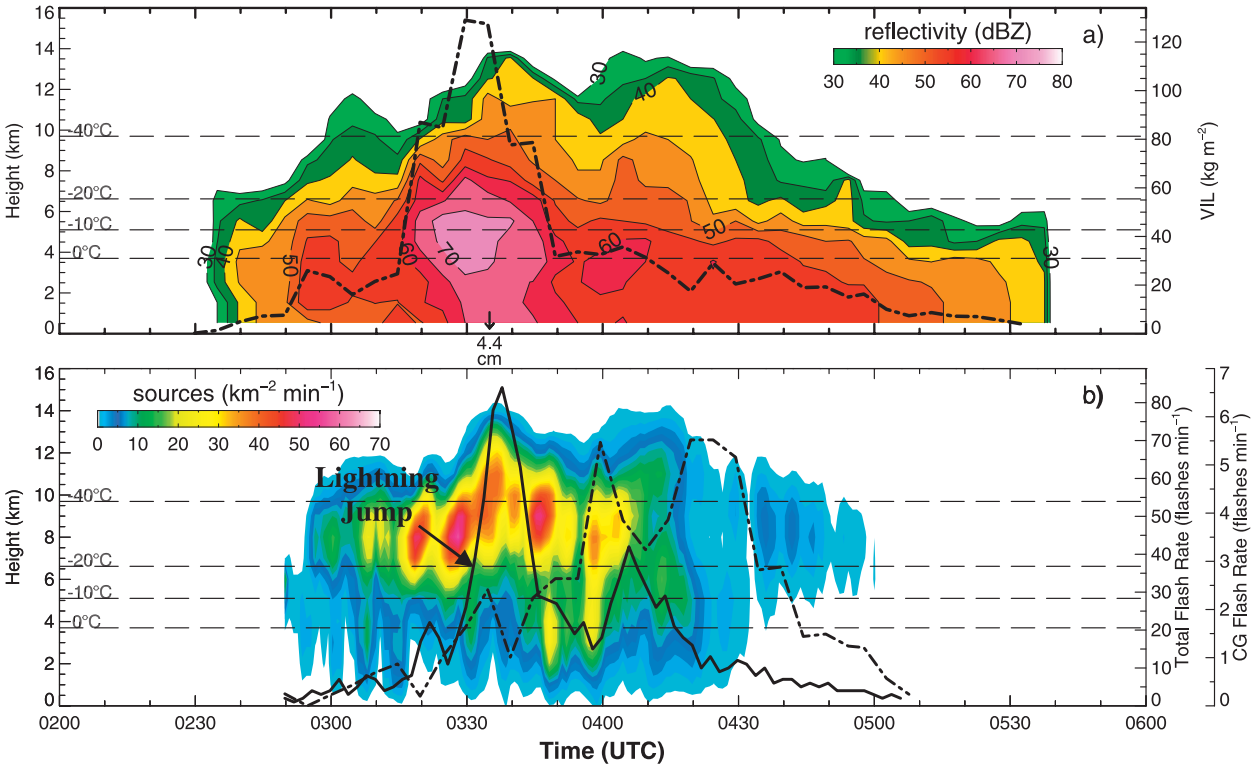

FIG. 4. Time–height evolution of (a) radar reflectivity (contours) with VIL (dash–dot line) and temperature (dashed lines). (b) VHF source density (contours) with 2-min total flash rate (i.e., flash rate averaged over a 2-min period; solid line) and 5-min CG flash rate (i.e., flash rate averaged over 5-min period; dash–dot line) from the nontornadic hail-producing thunderstorm on 30 Mar 2002.

strengthening of the updraft not only increases lightning activity but also stretches vertical vorticity. After the updraft surge, the vortex may take 15–25 min to descend to the ground (e.g., supercell tornadoes) or the vortex may develop quickly at all levels (e.g., nonsupercell tornadoes). Thus, the lightning jump should theoretically not provide as much advance notification of tornadogenesis for nonsupercell storms as it would for supercell storms.

4. Results of tests on the lightning jump algorithm

The 20 Tennessee Valley thunderstorms examined, including the two discussed in section 3, occurred during the spring months (March, April, and May) of 2002 and 2003. These thunderstorms collectively produced 110 severe weather events including 16 tornadoes, 81 hail events, and 9 straight-line winds events. Only one of the thunderstorms did not have any associated severe weather reports. In total, 15 of the 20 thunderstorms are supercell thunderstorms and the remaining are multicell and bow echo thunderstorms. In addition, 8 of the 20 thunderstorms were tornadic, and only 1 of these tornadic storms was not supercellular.

a. *Tornadic supercell*

The most prolific lightning-producing thunderstorm of the dataset occurred on 6 May 2003. This storm, cell C (Fig. 6), initiated in northern Mississippi, outside the domain of the LMA, and moved eastward across northern Alabama before transitioning to a bow echo at 1340 UTC in northeast Alabama and moving outside the LMA domain around 1500 UTC into northwest Georgia. This high precipitation (HP) supercell produced multiple tornadoes (one along its flanking line) and a peak 1-min total flash rate of 407 flashes min^{-1} as it tracked across northern Alabama.

At 1240 UTC, cell C resembled an HP supercell, (Moller et al. 1990), possessing a weak, broad rotational couplet (Fig. 6b) and bounded weak echo region (BWER) but no reflectivity hook echo. An inflow notch became apparent at 1255 UTC (not shown) as the supercell moved northeast of the NSSTC. A lightning hole, which is a region of relatively fewer or no lightning discharges occurring in the region of the rotating updraft (Lang et al. 2004), was observed for less than a 10-min period (at the same time as the radar observations shown in Fig. 6) with cell C and also corresponded with the location of the mesocyclone and BWER.

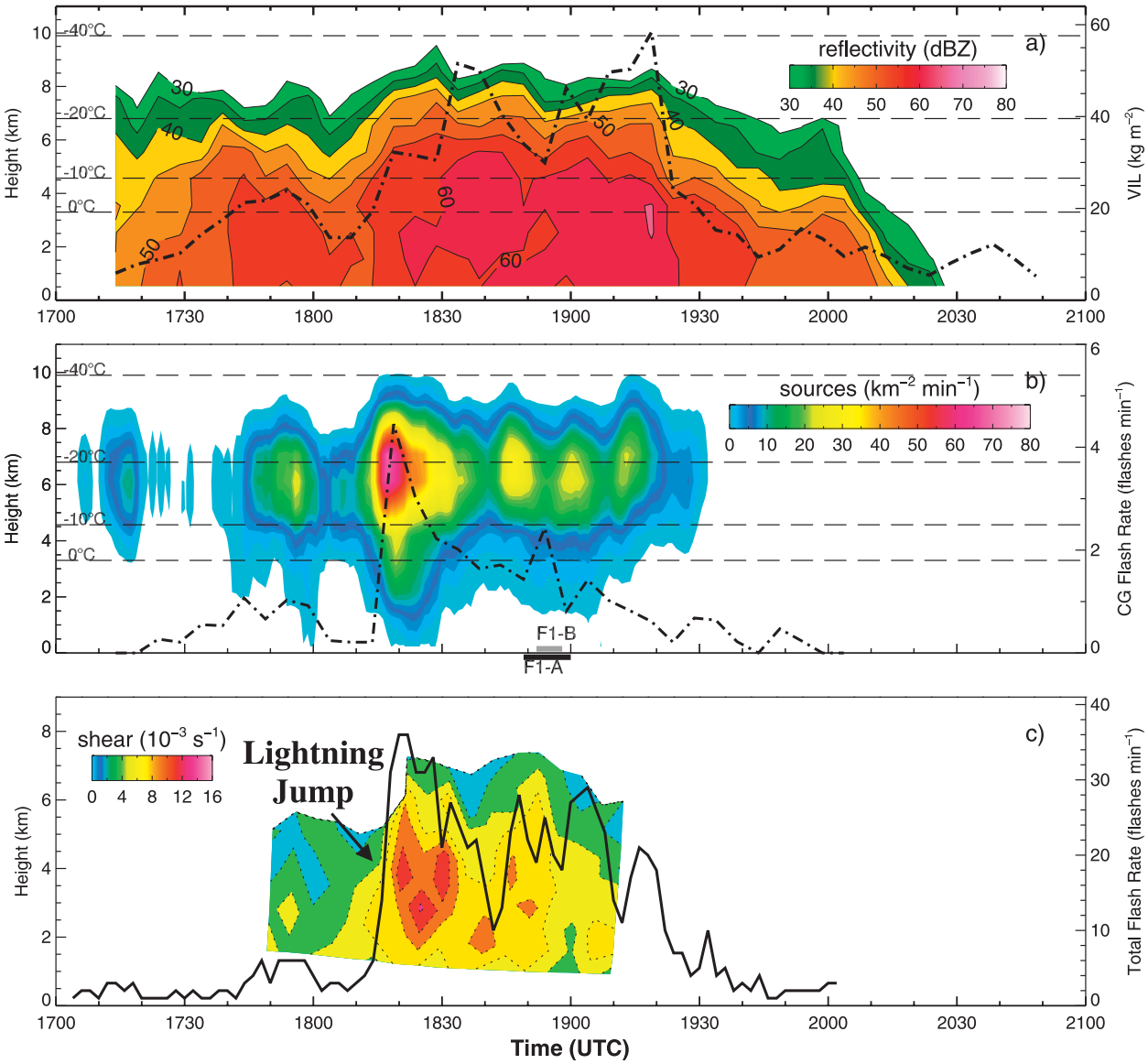

FIG. 5. Time–height series of (a) radar reflectivity with VIL (dash–dot line) and temperature (dashed lines), (b) VHF source density with 5-min CG flash rate, and (c) Doppler radar–derived radial shear with 2-min total flash rate from the tornadic "minisupercell" thunderstorm on 19 Mar 2003 in northeast Alabama.

The lightning history of this storm and its lightning jumps identified by the algorithm are shown in Fig. 7. The jump algorithm for this case was configured with a 10-min (5 samples) weighted moving average of the 2-min total flash rate (without removing singletons), 10-min weighted moving average of f', and a 6-min (3 samples) running average of the jump threshold. The algorithm was configured in this manner because it yields the best results for all 20 thunderstorm cases. The first severe weather report within the LMA domain occurred at 1115 UTC. It counts as a missed event using this algorithm configuration, but it is preceded by a jump in an algorithm configuration that used a 1-min total flash rate. At 1116 UTC, the algorithm identified the first lightning jump, 17 min prior to an F1 tornado. Another lightning jump was identified at 1156 UTC, followed by an F1 tornado at 1220 UTC. A larger lightning jump (11 flashes per minute squared; hereafter flashes min^{-2}) was identified at 1240 UTC followed 2 min later by hail, 18 min later by an F0 tornado, and 36 min later by an F1 tornado. This jump peaked at 184 flashes min^{-1} at 1246 UTC. Yet another jump was identified at 1316 UTC. Although this jump was only 2.7 flashes min^{-2}, the total flash rate remained above 150 flashes min^{-1}, and an

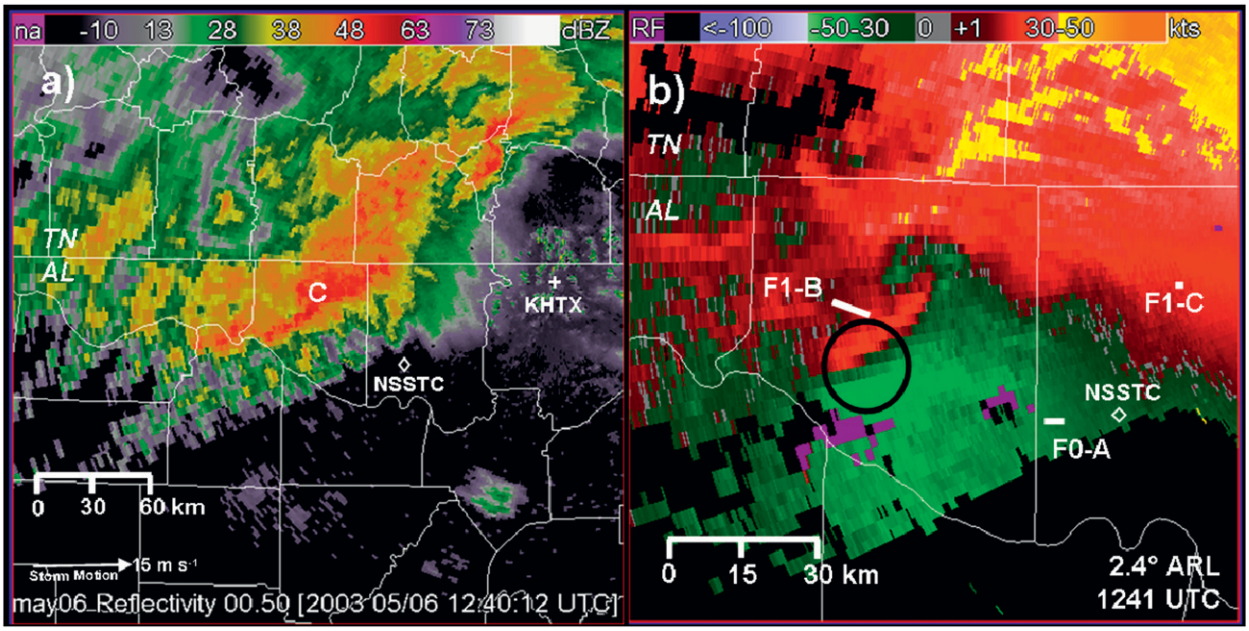

FIG. 6. KHTX radar images of the tornadic high-precipitation supercell at 1240 UTC 6 May 2003. (a) The 0.5° elevation scan of reflectivity (dBZ) and (b) the 2.4° elevation scan of storm relative velocity (kt) overlaid on county boundaries with the mesocyclone indicated by the circle and tornado tracks (bars). Storm motion is 15 m s^{-1} to the east.

F0 tornado occurred at 1345 UTC. Two more tornadoes were reported—an F0 at 1358 UTC and an F1 at 1413 UTC—but a jump is not identified within 30 min prior to either of these tornadoes. However, there is a final rapid increase in the total flash rate around 1330 UTC equaling that of the previous lightning jump. Figure 7 reveals that the jump threshold around 1330 UTC is just high enough (3 flashes min^{-2}) such that it could not be attained during this final increase in total flash rate. The final lightning jump identified before the storm exited the LMA domain occurred at 1450 UTC. Although this jump was only 1.2 flashes min^{-2}, it preceded a wind gust of 55 kt, which occurred at 1500 UTC.

The peak 2-min total flash rate and peak jump magnitude in Fig. 7 is less than the actual peak 1-min total flash rate (407 flashes min^{-1}) and jump magnitude (55 flashes min^{-2}) produced by the storm because of the type of algorithm configuration employed, which largely

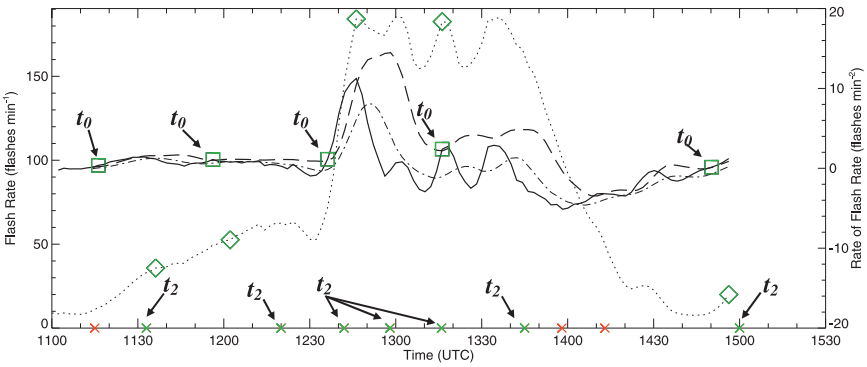

FIG. 7. The lightning jump threshold (f'_{thres}; dashed line) applied to the change in flash rate (f'; solid line) of the tornadic supercell, cell C, on 6 May 2003, to identify lightning jumps (squares) and their peak flash rate (diamonds). Lightning jumps that begin at time t_0 and precede severe weather occurrences at time t_2 are highlighted green (i.e., hits). Also shown is the 2-min total flash rate (f; dotted line) and moving average of f' ($\overline{f'}$; dash–dot line). Severe weather occurrences not preceded within 30 min by a lightning jump are highlighted as red (i.e., missed events).

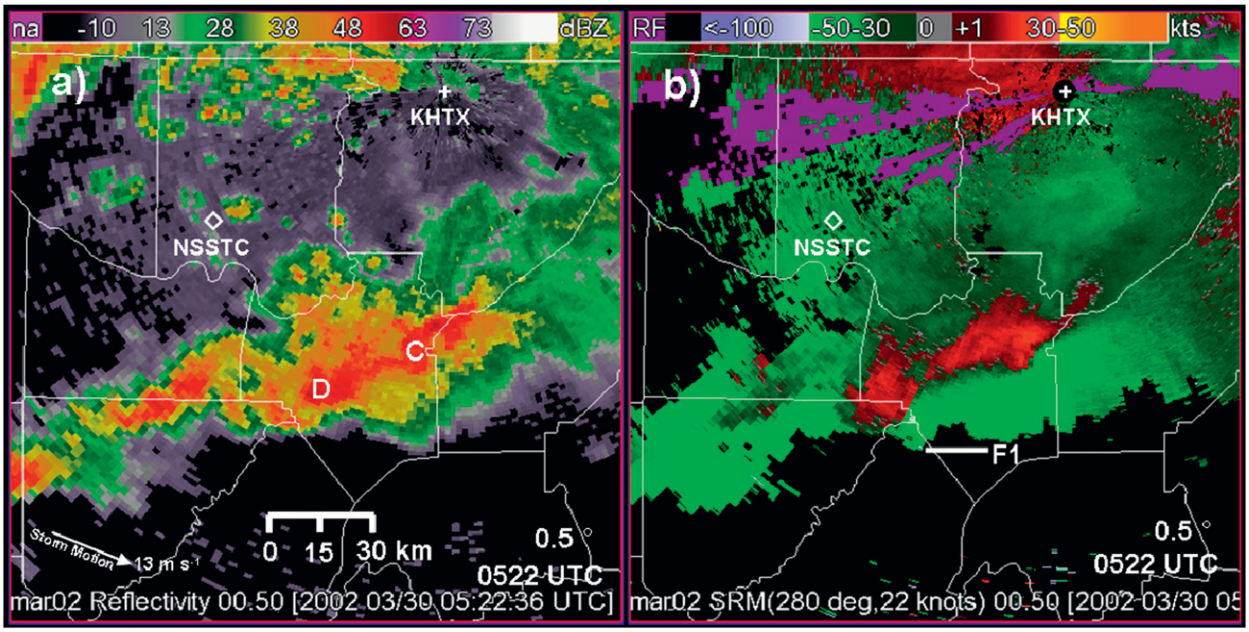

FIG. 8. Radar observations from KHTX at 0522 UTC 30 Mar 2002 of (a) 0.5° reflectivity (dBZ) and (b) 0.5° storm relative velocity (kt) overlaid on county boundaries. Cell D, a nonsupecell thunderstorm, produced the F1 tornado, whose track (bar) is annotated in (b). Storm motion is 13 m s^{-1} to the southeast.

dampened the extreme values of flash rate in an attempt to reduce the false alarms. This configuration of the jump algorithm resulted in seven hits, three missed events, and zero false alarms.

b. Tornadic nonsupercell

Identification of impending tornadic activity associated with nonsupercell storms can often be more difficult than identifying impending tornadic activity associated with supercell storms. However, the lightning jump algorithm can successfully provide advance indication of tornadic activity in nonsupercell thunderstorms. Figure 8 shows the radar reflectivity and storm relative velocity associated with a nonsupercell tornadic thunderstorm (cell D) that occurred on 30 March 2002 in northern Alabama. Environmental conditions were conducive to tornadic activity that day as moderate-to-high instability and high shear (CAPE values around 1200 J kg^{-1} and 0–3-km storm-relative helicity of 330 m^2 s^{-2}) were present across the region. This storm began as a multicellular cluster and evolved into a bow echo. It did exhibit a midlevel rotational couplet (Fig. 8b), similar to that of a mesocyclone, but the couplet was only detected for a brief 10-min period.

A time series of total lightning activity associated with this storm is shown in Fig. 9. The jump algorithm applied to this case was configured the same as that applied to the tornadic case discussed previously. The algorithm identified the first lightning jump at 0324 UTC, which preceded hail with 4.5-cm diameter observed at the surface by 11 min. The next two lightning jumps identified are at 0346 and 0408 UTC and both preceded severe weather occurrences. The jump at 0346 UTC was identified 24 min prior to a funnel cloud report and the jump at 0408 UTC identified 12 min prior to hail with a 5.1-cm diameter being observed at the ground. Since the total flash rate remains below 20 flashes min^{-1} through 0420 UTC, the magnitude of these lightning jumps is small (only 1 flash min^{-2}). Although the lightning jumps are small, there are distinct increases in the total flash rate associated with each jump identified before 0420 UTC. The lightning activity increased steadily after 0420 UTC, and the 40-dBZ reflectivity echoes grew to a height of 13.5 km AGL (not shown). At 0436 UTC, another lightning jump was identified, also with a magnitude of 1 flash min^{-2}. At 0450 UTC, 14 min later, another funnel cloud was reported. The total flash rate remained around 40 flashes min^{-1} after this jump until 0506 UTC, when another lightning jump was identified. This jump, which was 2 flashes min^{-2} in magnitude, occurred as the total flash rate increased to 60 flashes min^{-1} (see associated diamond in Fig. 8) and 14 min prior to an F1 tornado. The tornado began at 0520 UTC and persisted through 0535 UTC. During this time the total flash rate decreased to 42 flashes min^{-1}. After 0535 UTC, the total flash rate increased once again and the algorithm

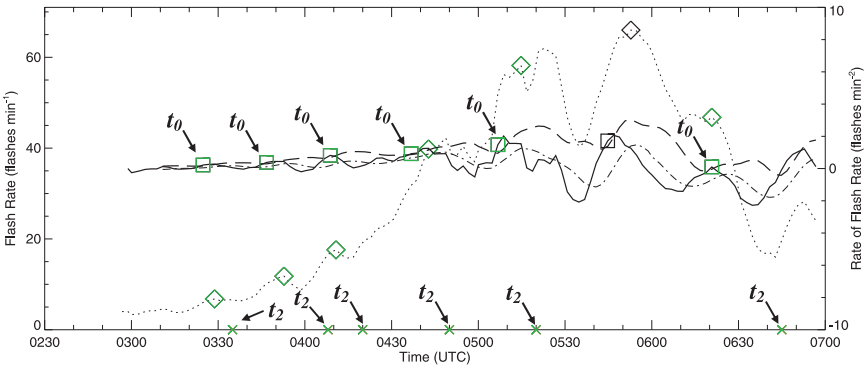

FIG. 9. Total lightning history of the tornadic, nonsupercell thunderstorm on 30 Mar 2002. The lightning jump threshold (f'_{thres}; dashed line) is applied to the change in flash rate (f'; solid line). Also shown is the 2-min total flash rate (f; dotted line) and moving average of f' ($\overline{f'}$; dash–dot line). Identified lightning jumps (squares) and their peak flash rate (diamonds) that begin at time t_0 and precede severe weather occurrences at time t_2 are highlighted green (i.e., hits).

identified a sixth lightning jump at 0544 UTC. Although this jump was also 2 flashes min^{-2} and the total flash rate peaked at 67 flashes min^{-2}, no severe weather was reported until 0645 UTC. However, this was outside the 30-min hit constraint discussed earlier, and thus the sixth lightning jump is a false alarm. The severe weather event at 0645 UTC did not occur without notification by the jump algorithm. There was one final lightning jump identified before the storm moved out of the LMA domain. The seventh jump was identified at 0620 UTC. It too had a magnitude less than 1 flash min^{-2}, but this jump did occur 25 min prior to 2.5-cm hail being reported on the ground.

The algorithm performed better for this case than the previous tornadic supercell case. The lightning jumps identified by the algorithm resulted in six hits, one false alarm, and zero missed events.

c. Nontornadic severe storm

A nontornadic severe hailstorm that occurred on 30 March 2002 was a left-moving storm resulting from a cell split that took place 50 km west of the NSSTC in northwest Alabama. Figure 10 shows the storm as viewed from the KHTX radar, after the split, in southern Tennessee at 0334 UTC. A three-body scatter spike in reflectivity (Lemon 1998) was present (Fig. 10a), and so was an elevated core of reflectivity exceeding 70 dBZ (Fig. 10b). This thunderstorm produced a peak 1-min total flash rate of 89 flashes min^{-1} and grew to a height near 17 km AGL. A lightning jump at 0322 UTC followed 13 min later by hail with a 4.4-cm diameter observed on the ground (see Fig. 11). This lightning jump occurred 4 min prior to the first appearance of a three-body scatter spike in the radar observations.

The peak 2-min total flash rate attained during the only jump identified with this algorithm configuration (same as applied to previously mentioned storms, which had no singletons removed) was 71 flashes min^{-1} (Fig. 11a). However, removing flashes containing fewer than 10 VHF sources resulted in a peak 2-min total flash rate of only 37 flashes min^{-1} and introduced a false alarm at 0410 UTC (Fig. 11b). Comparing the case without removing singletons from the defined flashes (Fig. 11a) and the case with flashes containing 10 or more VHF sources (Fig. 11b), we see that the trends are similar but much less amplified for the one in which singletons are removed. The smaller amplitude of the flash rate calculated from flashes containing at least 10 VHF sources resulted in a lower jump threshold relative to the algorithm run without a source constraint as well as a false alarm.

d. Nonsevere storm

The only nonsevere storm studied occurred on 30 March 2002 (cell B in Fig. 10). This storm initiated along a boundary that moved to the southeast across southern Tennessee. The jump algorithm was applied to this storm using both the 1- and 2-min total flash rates. The lightning history at both sampling rates is shown in Fig. 12. There was no smoothing performed on the 2-min configuration (Fig. 12a), but a 2-min moving averaging of the 1-min total flash rate was conducted on the 1-min configuration (Fig. 12b) in order to compare the differences between sampling rates given similar values of the flash rate. The trend in total flash rate is similar for the two sampling rates. Both produced a peak total flash rate of 51 flashes min^{-1} during a 40-min period (between 0250 and 0330 UTC) of relatively intense lightning activity. The lightning jump at 0400 UTC was identified

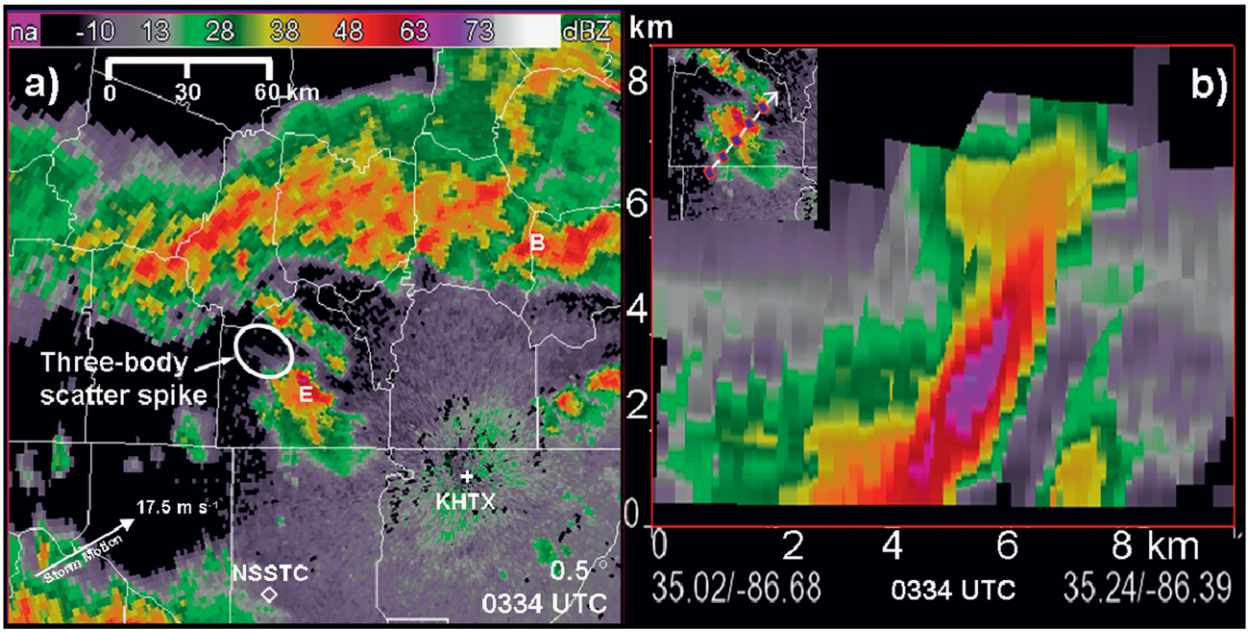

FIG. 10. Radar observations from KHTX near the Alabama/Tennessee border at 0334 UTC 30 Mar 2002, 2 min after the time of peak electrical activity of cell E. (a) The 0.5° radar elevation scan of reflectivity (dBZ) overlaid on county boundaries and (b) reconstructed vertical cross section (i.e., images of plan position indicator views are stitched together) of cell E reflectivity along the dashed arrow (see inset) between 0 and 8 km above radar level. The ellipse annotated in (a) is the first appearance of the three-body scatter spike at the lowest elevation scan. Storm motion of cell E is 17.5 m s^{-1} to the northeast.

using both sampling rates but is much more pronounced (i.e., larger) in the 1-min rate storm shown in Fig. 12b. This jump attained 15 flashes min^{-2} using a 1-min sampling rate, whereas the jump identified with a 2-min sampling rate reached only 4 flashes min^{-2}. Minor fluctuations of the flash rate are far more pronounced in the 1-min configuration (Fig. 12b), which triggered the jump threshold more often and resulted in nearly twice as many lightning jumps being identified.

So in summary, the 1-min configuration resulted in five false alarms, whereas the 2-min configuration resulted in only three false alarms. Since there was no severe weather reported with this storm, the 2-min configuration yielded better results than the 1-min configuration.

e. Algorithm performance

The lightning jump algorithm described above was tested on 20 thunderstorms (19 severe and 1 nonsevere) that occurred within the North Alabama LMA domain. Lightning jumps identified during the sensitivity tests on the algorithm framework preceded severe weather by a mean of 18 min. The highest CSI was attained using the following combination of parameters: 1) a 2-min total flash rate (without removing singletons), 2) a 10-min running average of the 2-min total flash rate, 3) a 10-min running average of the change in flash rate, 4) a 6-min running average of the jump threshold, and 5) the mean and standard deviation of the change in flash rate were calculated over a 12-min period. The lightning jumps identified by this configuration of the jump algorithm and classified as hits (i.e., they preceded severe weather) are listed in Table 1. A total of 67 lightning jumps were identified, and 41 of these preceded severe weather by an average of 22 min. Two of these jumps were identified prior to a severe weather event, but they are not counted in the total number of hits (and not included in Table 1) because a prior lightning jump had occurred within 30 min of the severe weather event. Thirty-nine of the lightning jumps, which attained a mean peak 2-min total flash rate of 60 flashes min^{-1} (note that peak flash rate is the maximum total flash rate attained during the jump and not the storm maximum total flash rate) with an average jump magnitude of 2 flashes min^{-2}, are counted as hits. In contrast, 26 lightning jumps, which attained a mean peak total flash rate of only 30 flashes min^{-1} with an average jump magnitude of 1.4 flashes min^{-2}, did not precede any severe weather events within 30 min (i.e., false alarms). Fourteen severe weather events were not preceded by lightning jumps using this 2-min configuration. Thus, the performance measures of this algorithm configuration for the 20 thunderstorms are a POD of 0.74, FAR of 0.40, and CSI of 0.49. Furthermore the mean lead time provided by the lightning jumps identified with this algorithm configuration is 22 min.

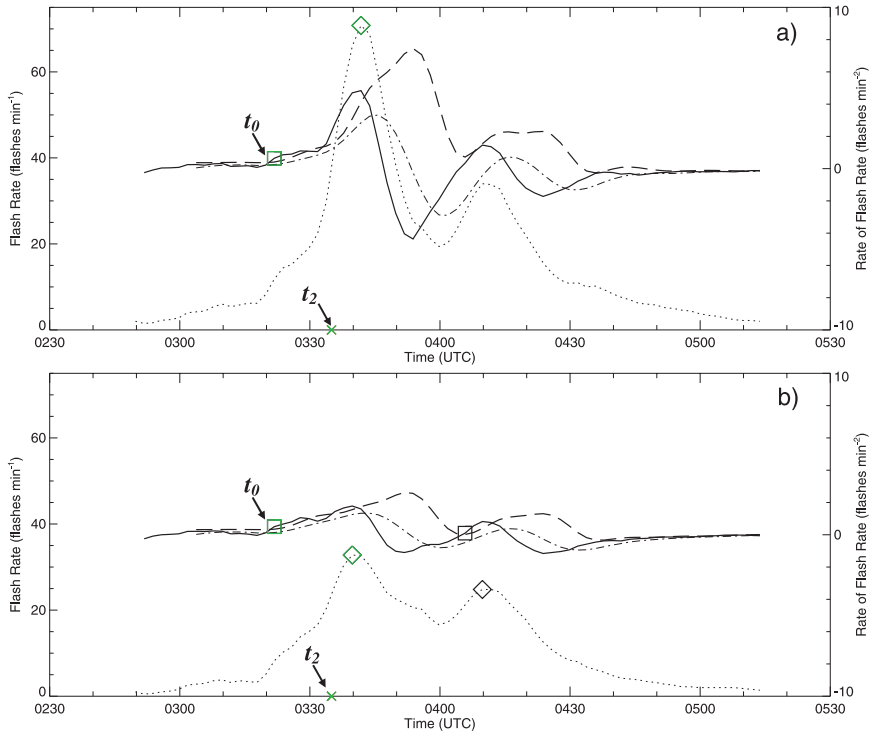

FIG. 11. The lightning jump threshold (f'_{thres}; dashed line) is applied to the change in flash rate (f'; solid line) of the nontornadic severe thunderstorm on 30 Mar 2002. Two algorithm configurations are shown: the 2-min total flash rate (f; dotted line) calculated from (a) flashes with no singletons removed and (b) flashes containing at least 10 VHF sources. Also shown is the moving average of f' ($\overline{f'}$; dash–dot line). Identified lightning jumps (squares) and their peak flash rate (diamonds) that begin at time t_0 and precede severe weather occurrences at time t_2 are hits (highlighted green).

The highest POD (=0.90) was attained by configuring the algorithm with the following combination of parameters: 1) a 1-min total flash rate (without removing singletons), 2) a 5-min moving average of the 1-min total flash rate, 3) a 5-min moving average of the change in flash rate, 4) a 5-min weighted moving average of the jump threshold, and 5) the mean and standard deviation of the change in flash rate were calculated over a 10-min period. However, since the higher sampling rate (1-min total flash rate) employed in this configuration was more "sensitive" to minor fluctuations in the total flash rate, it also yielded the highest FAR (=0.60). Table 2 shows the results of this 1-min configuration, as well as the 2-min configuration for comparison. The mean peak 1-min flash rate attained during each lightning jump classified as a hit is 70 flashes min^{-1} with a mean jump magnitude of 4.8 flashes min^{-2}. The lightning jumps classified as false alarms attain a mean peak total flash rate of only 30 flashes min^{-2}, half that attained by lightning jumps classified as hits. The mean jump magnitude of the false alarms is 2 flashes min^{-2}, also half that attained by the hits. Lightning jumps identified by this 1-min algorithm configuration preceded severe weather by a mean of 18 min. The 1-min configuration resulted in more hits, a higher mean peak flash rate and higher jump magnitude, but the jumps identified by the 2-min configuration yielded 20 fewer false alarms as well as a 4-min longer lead time.

5. Discussion

An algorithm was developed to identify precursory signatures, referred to as lightning jumps, in the total lightning activity of thunderstorms to be used as in indication of impending severe weather. Using the North Alabama LMA and flash algorithm, this lightning jump algorithm was tested on 20 thunderstorms that occurred during the spring months of 2002 and 2003 across northern Alabama and southern Tennessee.

Seven of the eight tornadic thunderstorms exhibited supercellular characteristics. The supercell, which produced the highest total flash rate (1-min total flash rate of 407 flashes min^{-1}), also spawned the most tornadoes. The lightning jump algorithm identified 4 lightning

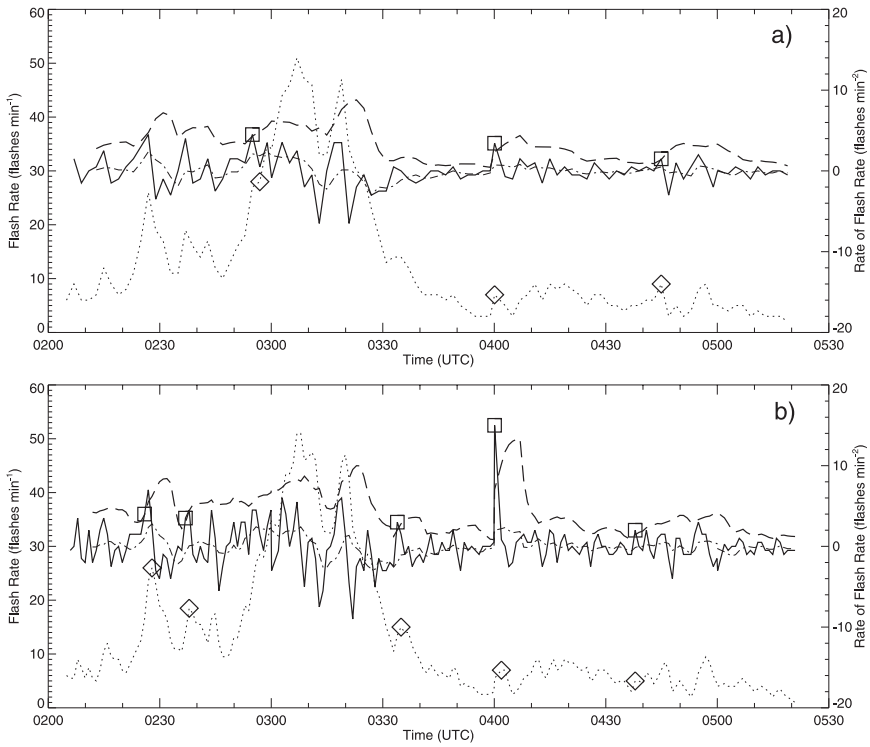

FIG. 12. Comparison of two different lightning jump algorithm configurations using the total lightning history of the nonsevere thunderstorm on 30 Mar 2002. The algorithm was configured with a (a) 2-min total flash rate (dotted line) and (b) 1-min total flash rate (dotted line) used to calculate the change in flash rate (f'; solid line), jump threshold (f'_{thres}; dashed line), and moving average of f' ($\overline{f'}$; dash–dot line). Also shown are lightning jumps identified (squares) and their peak total flash rate (diamonds). Since no severe weather events were reported with this storm, all the jumps identified are counted as false alarms, and hence are not highlighted green.

jumps in this storm, which preceded six of the eight tornadoes by an average of 18 min. This high precipitation supercell also exhibited a lightning jump of 55 flashes min^{-2}, the largest lightning jump detected in this study, and it occurred during a relatively long track F1 tornado (on the ground for 22 min). Once the tornado ended, the lightning jump peaked, and hail with a 2.2-cm diameter was observed at the ground. The trend in lightning activity during the 22-min-long F1 tornado (within 9 min the 1-min total flash rate increased from 77 to 380 flashes min^{-1}) is indicative of rapid updraft intensification within the mixed-phase region of the storm, which then likely enhanced hydrometeor growth. This was then followed by an intensifying downdraft below the mixed-phase region, which cut off the tornado's inflow and resulted in the hail reported on the ground.

Both 1- and 2-min total flash rates were tested with the jump algorithm. The 1-min total flash rate tests resulted in the most numerous detections of lightning jumps preceding severe weather (POD = 0.90), but the 1-min total flash rate tests also identified the most number of lightning jumps not followed by severe weather (FAR = 0.60). Tests conducted with the 2-min total flash rate yielded the lowest FAR (=0.34), but the POD was 15% lower than that of the 1-min sampling rate. The high false alarm rate, especially for the 1-min lightning activity, can be partly attributable to sensitivity of the jump threshold to small fluctuations in the total flash rate that otherwise are less pronounced at lower sampling rates of lightning activity. Another possibility for the high FAR can be attributed to the strict definition of severe weather for wind and hail events or simply the lack of severe weather reports associated with a storm. There may have been hail or wind events that occurred but were just below severe weather criteria (e.g., microburst storm in Goodman et al. 1988) and thus not included in *Storm Data*.

The peak 1- and 2-min total flash rates (without removing singletons) of 14 Tennessee Valley thunderstorms with lightning jumps prior to severe weather exceeded 60 flashes min^{-1}. Thereby, the majority of the storms in this dataset tend to separate themselves into severe and nonsevere based solely upon peak total flash rate, as was found to be the case with the Florida

TABLE 1. Lightning jumps identified as hits at time t_0 with a peak at t_1 before severe weather at time t_2. Tornado events are indicated by their Fujita-scale classification. Mean/max/min: 60/184/3 (peak flash rate) and 2.3/11.2/0.8 (jump magnitude). Average lead time ($t_2 - t_0$): 22 min.

Storm (Date–cell)	Peak flash rate (Flashes min^{-1})	Jump magnitude (Flashes min^{-2})	t_0 (UTC)	t_1 (UTC)	t_2 (UTC)	Severe weather Hail (H; in.) and wind (W; kt)
30 Mar 2002–A	23	0.9	0309	0315	0340	H-0.88
30 Mar 2002–C	24	0.2	0309	0309	0335	H-0.75
30 Mar 2002–C	56	1.1	0431	0431	0456	Funnel cloud
30 Mar 2002–C	35	1.8	0507	0513	0530	H-0.88
30 Mar 2002–D	7	0.3	0325	0329	0335	H-1.75
30 Mar 2002–D	12	0.4	0347	0353	0408	Funnel cloud
30 Mar 2002–D	18	0.8	0409	0411	0420	H-2
30 Mar 2002–D	40	1.3	0437	0443	0450	Funnel cloud
30 Mar 2002–D	58	2.0	0507	0515	0520	F1
30 Mar 2002–D	47	0.1	0621	0621	0645	H-1
30 Mar 2002–E	71	4.8	0322	0342	0335	H-1.75
28 Apr 2002–D	67	1.8	2022	2030	2030	H-1.75 (F0–2042 UTC)
28 Apr 2002–D	77	1.1	2110	2110	2139	H-0.75
28 Apr 2002–D	60	2.0	2146	2158	2205	H-0.75
28 Apr 2002–E	40	1.6	2014	2030	2045	H-1
19 Mar 2003–B	15	0.2	1832	1834	1842	F1, W-70
19 Mar 2003–D	33	2.7	1818	1828	1849	F1, F1
19 Mar 2003–E	3	0.1	1756	1804	1815	H-0.75
19 Mar 2003–G	34	2.2	1948	1958	1957	F0
2 May 2003–A	82	6.6	1831	1845	1855	H-1.75
2 May 2003–F	84	5.9	1903	1917	1920	H-0.75
2 May 2003–F	93	4.0	1947	1949	1950	H-1.75
2 May 2003–G	33	1.6	1936	1948	1950	H-2.75
2 May 2003–G	61	2.2	1954	2004	2030	H-1.75
2 May 2003–H	146	6.6	2024	2034	2050	H-1.75
2 May 2003–H	80	0.1	2102	2100	2106	H-1, 1.75
2 May 2003–I	58	2.4	2029	2051	2055	H-1
2 May 2003–J	70	3.4	2016	2018	2040	H-1.75
2 May 2003–J	146	3.9	2046	2110	2052	H-0.75, 2
2 May 2003–J	103	2.1	2206	2212	2222	H-0.75, W-55
2 May 2003–J	62	0.2	2256	2260	2317	W-50, H-0.75
5 May 2003–A	47	2.6	1510	1522	1547	H-1, F0
5 May 2003–A	44	1.9	1556	1606	1618	H-4.5
5 May 2003–A	72	2.6	1626	1636	1635	W-55, 80 (F3–1645)
6 May 2003–C	36	1.4	1116	1136	1133	F0, F1
6 May 2003–C	53	1.1	1156	1202	1220	F1
6 May 2003–C	184	11.2	1236	1246	1242	H-0.88 (F0–1258)
6 May 2003–C	183	2.7	1316	1316	1345	F0
6 May 2003–C	20	1.2	1450	1456	1500	W-55

thunderstorms in Williams et al. (1999). However, unlike the severe cases of Williams et al. (1999), in which all of the severe storms produced peak 1-min total flash rates of at least 60 flashes min^{-1}, four of the severe storms in the dataset presented here produced peak 1-min total flash rates less than 60 flashes min^{-1}. With the exception of one multicellular storm, the severe storms with less than 60 flashes min^{-1} peak total flash rates were minisupercell thunderstorms. The 30-dBZ reflectivity echo associated with these minisupercells did not exceed 10–12 km AGL, whereas the 30-dBZ reflectivity echo of the other severe thunderstorms in the dataset grew to a height of at least 14 km AGL. The radial constraint of 10–15 km was large enough to capture the vast majority of all flashes produced by each minisupercell. Thus, the difference in vertical extent (~2–4 km) between the minisupercell severe storms and the other severe storms could partially explain the peak total flash rate difference for severe storms presented here and those in Williams et al. (1999). Regardless of storm height, the algorithm developed in this study successfully identified the less electrically active minisupercell storms as severe, based solely upon the trends in lightning activity.

Since storm intensity is governed by updraft strength, it follows that an F3 tornado and 10-cm (4 in.) hail would

TABLE 2. Lightning activity statistics taken from the lightning jump algorithm configurations that yielded the highest critical success index for both the 1- and 2-min total flash rates. The number of hits and false alarms are contained within parenthesis by their respective sampling rates.

	Peak flash rate Min/max/mean (Flashes min^{-1})	Jump magnitude Min/max/mean (Flashes min^{-2})	Lead time Min/max/mean (Min)
Hits			
1 min (45)	3/386/70	0.4/31.5/4.8	1/42/18
2 min (39)	3/184/60	0.1/11.2/2.3	3/51/22
False alarms			
1 min (46)	1/85/30	0.2/6.6/2.4	N/A
2 min (26)	2/91/30	0.1/4.7/1.4	N/A

be associated with a higher total flash rate than a storm that produced only an F0 tornado and 2.5-cm (1 in.) hail. Thus, we would expect to find a positive correlation between total flash rate and severe weather intensity. However, no significant correlation was found between tornado intensity (F0 versus F3), hail diameter, or wind speed and peak total flash rate, lightning jump magnitude, or lead time. This conflict may partially be due to the lack of intense tornadoes included in this study (only 1 of the 16 tornadoes exceeded F2 intensity).

Since the 2-min sampling rate yielded the highest CSI, it was also used to test the sensitivity of the jump algorithm to the definition of a flash (i.e., number of VHF sources detected by the LMA used to define a flash). The magnitude of the lightning jumps and the peak total flash rate attained during a jump were reduced as the flash definition became more constraining (i.e., removing 5, 10, and 30 source flashes). However, the overall trends in total flash rate were similar regardless of the minimum source constraint imposed on the flash definition. Furthermore, there is no trend in POD, FAR, nor CSI as the flash definition was increased from 0 to 30 sources. For instance, the highest POD attained in the 0 source constraint was 0.75, but it was 0.73 for the 10 source constraint and 0.80 for the 30 source constraint. The lowest FAR attained was 0.24 in the 10 source constraint but it was 0.34 for the 0 source constraint and 0.36 for the 30 source constraint. Thus, there seems to be no real dependency of POD or FAR on flash definition. This result was expected since the total flash rate trends remained virtually unchanged as the source constraint was increased.

The lightning algorithm performance is better than the NEXRAD algorithms used operationally to identify severe weather. The tornado detection algorithm, which detects tornado vortex signatures in velocity, only has a POD of 0.37, FAR of 0.78, and CSI of 0.16 (Mitchell et al. 1998). The mesocyclone detection algorithm, which detects storm rotation, has a POD of 0.53, FAR of 0.73, and CSI of 0.22 in prediction of tornadoes and 0.40, 0.66, and 0.22 in prediction of severe wind events algorithm (Stumpf et al. 1998). The hail detection algorithm, which relates high reflectivity values to hail size, has a POD of 0.78, FAR of 0.69, and CSI of 0.29 (Witt et al. 1998a). Although these algorithms are radar based, they are the only ones that are available to the operational forecaster to predict impending severe weather and also are the only severe weather algorithms whose statistics are available in the literature for comparison. These results suggest that the addition of lightning jump identification to any of these NEXRAD severe weather algorithms would likely improve their performance statistics.

6. Conclusions

Since total lightning activity tends to follow the trend in updraft, rapid increases in the total flash rate are indicative of updraft intensification. These rapid increases in total flash rate, termed lightning jumps, have been observed to occur as severe weather manifests within the storm. As a result, the lightning jumps have been successfully used to diagnose thunderstorm intensity (severe or nonsevere). The total lightning algorithm developed in this study, the first quantitative algorithm of its kind, successfully exploits the link among updraft, lightning, and severe weather by objectively identifying lightning jumps, which can then be used to diagnose thunderstorm intensity and to predict the potential for severe weather.

The lightning jump algorithm developed here successfully identified rapid increases in the total lightning activity in advance of severe weather events produced by 20 thunderstorms. Performance of the algorithm varied depending upon how the lightning data were sampled and processed. The 2-min sampling rate of the total lightning activity (i.e., 2-min average) yielded the best results (high POD, low FAR, and longest lead time). The 2-min sampling rate provided, on average, a 22-min advance notification of severe weather. In contrast, a 1-min total flash rate yielded a lead time of 18 min and resulted in a 26% higher FAR.

The effects of altering the lightning flash definition (i.e., with or without singletons) has minimal effect on this algorithm's performance when using a 2-min sampling rate of total lightning activity. However, it does affect the total flash rate and jump magnitude. Thus, caution should be exercised if the jump threshold is altered and based upon any unique value of the flash rate or jump magnitude when using a VHF lightning mapping system to detect and define lightning flashes. The results of this study suggest that when using lightning as an indicator or predictor of severe weather, it is not any one flash rate that is important but yet the trend in the flash rate of a storm evolving in an environment favorable for severe weather. Any "magic" flash rate threshold value may cause some severe storms to go unwarned based upon lightning data alone. Perhaps a new parameter/index could be derived from total flash rate and also include cloud-top height and/or vertically integrated liquid.

The total lightning diagnostic tool developed here yields promising results for determining thunderstorm intensity. Since the only input into the algorithm is flash rate, the algorithm can easily be tested on thunderstorm datasets collected with other ground-based lightning systems as well as lightning observations from future geostationary satellites, such as GOES-R. However, additional testing of this algorithm is warranted, especially on a dataset including a greater number of nonsevere thunderstorms. One such study by Schultz et al. (2009) has already built upon our results and demonstrated even better statistical performance of the algorithm concept across a broader range of storm types. Together these studies provide a foundation for the implementation of future lightning jump algorithms on platforms, such as GOES-R. Algorithm refinement is also needed in order to reduce the number of identified lightning jumps that are not followed by severe weather (i.e., false alarms). It must be kept in mind though that simply adjusting the jump threshold to decrease the FAR will also decrease the POD. Integration of additional datasets (e.g., storm environmental parameters, radar observables, satellite cloud-top observations, other severe weather algorithms, etc.) into this thunderstorm intensity algorithm would likely result in the best improvement to critical success index and lead time.

The examination of trends in total flash rate, which this algorithm performs objectively, should compliment the radar and will be of the most help when radar signatures are vague or not apparent (e.g., nonsupercell tornadoes, microbursts, etc.). In the event of a radar outage, the lightning jumps may be the only indication of severe weather. NWS warning forecasters already have an abundance of information to digest in the warning decision-making process, and the lightning jump algorithm could alleviate some of that burden and thereby increase warning lead time.

Acknowledgments. Funding for this research was provided by the NASA SMD's Earth Science Division in support of the Short-term Prediction and Research Transition (SPoRT) program at Marshall Space Flight Center and by the NOAA/NESDIS GOES-R Program office. The authors thank Dr. Richard Blakeslee, John Hall, Jeff Bailey, and Sam Acoff for maintaining and processing the North Alabama Lightning Mapping Array and its output. Dr. Eugene "Bill" McCaul Jr. provided lightning flash data from the source clustering "flash" algorithm. We are grateful to Chris Darden and the local NWS weather forecast office in Huntsville, Alabama, for the collaboration and feedback they have provided on the operational utility of total lightning data and the lightning jump signature. The authors would also like to thank Dr. Earle Williams for his helpful comments and thorough review of this paper, as well as those of the anonymous reviewers. The views, opinions, and findings contained herein are those of the authors, and should not be construed as an official NASA, NOAA, or U.S. government position, policy, or decision.

APPENDIX

The Jump Threshold in the Lightning Jump Algorithm

By design, the jump threshold is updated with each new sample of lightning activity, and its components (mean and standard deviation) are based upon the past N number of samples. This results in a moving threshold that can be tuned to be less sensitive to minor fluctuations in the total flash rate that may increase the FAR. This backward-moving average threshold f'_{thres} is given by

$$f'_{\text{thres}}(t) = \frac{\overline{f'(t)} + 2\sigma[f'(t)] + f'_{\text{thres}}(t-1)}{2}, \quad \text{(A1)}$$

where $\overline{f'(t)}$ and $\sigma[f'(t)]$ are the moving average and standard deviation of the change in flash rate, respectively, and are given by

$$\overline{f'(t)} = \frac{1}{N}\sum_{t=t-N}^{t} f'(t), \quad \text{(A2)}$$

$$\sigma[f'(t)] = \sqrt{\frac{1}{N}\sum_{t=t-N}^{t}[f'(t) - \overline{f'(t)}]^2}, \quad \text{(A3)}$$

in which N is the number of samples before the current time t used to calculate the mean and standard deviation. For example, if $N = 10$ and the sampling rate of the flash rate is every 2 min (i.e., total flash rate averaged over a 2-min period), then the mean and standard deviation would be calculated over a 20-min period.

However, decreasing the sensitivity of the jump threshold can also result in a corresponding decrease in detection of lightning jumps. Thus, to provide more emphasis on shorter-term trends of the total flash rate while retaining some influence from previous changes in total flash rate, a weighted moving average of the jump threshold is calculated. This is accomplished by including a weighting factor:

$$w_t = \frac{t - N}{N}, \tag{A4}$$

which, depending upon algorithm configuration, can be applied to the total flash rate, its derivative, or the jump threshold, such as

$$f'_{\text{thres}}(t) = \frac{1}{N} \sum_{t=t-N}^{t} f'_{\text{thres}}(t)\, w_t. \tag{A5}$$

The weighting factor w_t is linear and dependent upon the number of samples N used in the moving average. This linear weighting factor gives the most amount of weight to the current sample t and the least amount of weight to the oldest sample $t - N$. For example, if the total flash rate is averaged over 2 min ($\Delta t = 2$) and three samples ($N = 3$) are used to calculate the weighted moving average of the jump threshold, then $w_t = 1/3$, $2/3$, and 1 at times $t - 2\Delta t$, $t - \Delta t$, and at the current time t, respectively.

Similar smoothing techniques (i.e., moving average and weighted moving average) were also applied to the total flash rate and the change in total flash rate. Along with the various smoothing techniques (sample size and standard or weighted moving average), the temporal resolution of the flash rate (e.g., 1 or 2 min) and the number of singletons removed from a flash, there are a total of five parameters used to configure the jump algorithm and these parameters are explained in section 2c.

REFERENCES

Baker, M. B., H. J. Christian, and J. Latham, 1995: A computational study of the relationships linking lightning frequency and other thundercloud parameters. *Quart. J. Roy. Meteor. Soc.,* **121,** 1525–1548.

——, A. M. Blyth, H. J. Christian, A. M. Gadian, J. Latham, and K. Miller, 1999: Relationships between lightning activity and various thundercloud parameters: Satellite and modeling studies. *Atmos. Res.,* **51,** 221–236.

Burgess, D. W., R. R. Lee, S. S. Parker, D. L. Floyd, and D. L. Andra Jr., 1995: A study of mini supercells observed by WSR-88D radars. Preprints, *27th Conf. on Radar Meteorology,* Vail, CO, Amer. Meteor. Soc., 4–6.

Cummins, K. L., M. J. Murphy, E. A. Bardo, W. L. Hiscox, R. B. Pyle, and A. E. Pifer, 1998: A combined TOA/MDF technology upgrade of the U.S. National Lightning Detection Network. *J. Geophys. Res.,* **103,** 9035–9044.

——, J. A. Cramer, C. J. Biagi, E. P. Krider, J. Jerasuld, M. A. Uman, and V. A. Rakov, 2006: The U.S. National Lightning Detection Network: Post-upgrade status. Preprints, *Second Conf. on Meteorological Applications of Lightning Data,* Atlanta, GA, Amer. Meteor. Soc., 6.1.

Darden, C. B., P. Gatlin, J. Burks, S. Goodman, D. E. Buechler, and J. M. Hall, 2006: Total lightning in the warning decision making process—Two years of case studies. Preprints, *Second Conf. on Meteorological Applications of Lightning Data,* Atlanta, GA, Amer. Meteor. Soc., 1.1.

Deierling, W. K., 2006: The relationship between total lightning and ice fluxes. Ph.D. dissertation, University of Alabama in Huntsville, 175 pp.

Demetriades, N. W. S., D. E. Buechler, C. B. Darden, G. R. Patrick, and A. Makela, 2008: VHF total lightning mapping data use for thunderstorm nowcasting at weather forecast offices. Preprints, *Third Conf. on Meteorological Applications of Lightning Data,* New Orleans, LA, Amer. Meteor. Soc., 8.5.

Goodman, S. J., D. E. Buechler, P. D. Wright, and W. D. Rust, 1988: Lightning and precipitation history of a microburst-producing storm. *Geophys. Res. Lett.,* **15,** 1185–1188.

——, and Coauthors, 2005: The North Alabama Lightning Mapping Array: Recent severe storm observations and future prospects. *Atmos. Res.,* **76,** 423–437.

——, R. Blakeslee, D. Boccippio, H. Christian, W. Koshak, and W. A. Petersen, 2006: GOES-R Lightning Mapper (GLM) research and applications risk reduction. Preprints, *Second Symp. Toward a Global Earth Observation System of Systems–Future National Operational Environmental Satellite Systems,* New Orleans, LA, Amer. Meteor. Soc., 2.2.

Greene, D. R., and R. A. Clark, 1972: Vertically integrated liquid water—A new analysis tool. *Mon. Wea. Rev.,* **100,** 548–552.

Hondl, K., 2002: Current and planned activities for the warning decision support system-integrated information (WDSS-II). Preprints, *21st Conf. on Severe Local Storms,* San Antonio, TX, Amer. Meteor. Soc., 4.8.

Kennedy, P. C., N. E. Westcott, and R. W. Scott, 1993: Single-Doppler observations of a mini-supercell tornadic thunderstorm. *Mon. Wea. Rev.,* **121,** 1860–1870.

Kingsmill, D. E., and R. M. Wakimoto, 1991: Kinematic, dynamic, and thermodynamic analysis of a weakly sheared severe thunderstorm over northern Alabama. *Mon. Wea. Rev.,* **119,** 262–297.

Koshak, W. J., and Coauthors, 2004: North Alabama Lightning Mapping Array (LMA): VHF source retrieval algorithm and error analysis. *J. Atmos. Oceanic Technol.,* **21,** 543–558.

Lang, T. J., and Coauthors, 2004: The Severe Thunderstorm Electrification and Precipitation Study. *Bull. Amer. Meteor. Soc.,* **85,** 1107–1125.

Lemon, L. R., 1998: The radar "three-body scatter spike": An operational large-hail signature. *Wea. Forecasting,* **13,** 327–340.

MacGorman, D. R., D. W. Burgess, V. Mazur, W. D. Rust, W. L. Taylor, and B. C. Johnson, 1989: Lightning rates relative

to tornadic storm evolution on 22 May 1981. *J. Atmos. Sci.,* **46,** 221–250.

McCaul, E. W., Jr., J. Bailey, J. Hall, S. J. Goodman, R. J. Blakeslee, and D. E. Buechler, 2005: A flash clustering algorithm for North Alabama Lightning Mapping Array data. Preprints, *Conf. on Meteorological Applications of Lightning Data,* San Diego, CA, Amer. Meteor. Soc., 5.2.

——, S. J. Goodman, K. M. LaCasse, and D. J. Cecil, 2009: Forecasting lightning threat using cloud-resolving model simulations. *Wea. Forecasting,* **24,** 709–729.

Mitchell, E. D., S. V. Vasiloff, G. J. Stumpf, A. Witt, M. D. Eilts, J. T. Johnson, and K. W. Thomas, 1998: The National Severe Storms Laboratory Tornado Detection Algorithm. *Wea. Forecasting,* **13,** 352–366.

Moller, A. R., C. A. Doswell III, and R. Przbylinksi, 1990: High-precipitation supercells: A conceptual model and documentation. Preprints, *16th Conf. on Severe Local Storms,* Kananaskis Park, AB, Canada, Amer. Meteor. Soc., 52–57.

Oye, D., and M. Case, 1995: REORDER: A program for gridding radar data. Installation and use manual for the UNIX version. NCAR Atmospheric Technology Division, 19 pp.

——, C. Mueller, and S. Smith, 1995: Software for radar translation, visualization, editing, and interpolation. Preprints, *27th Conf. on Radar Meteorology,* Vail, CO, Amer. Meteor. Soc., 359–361.

Proctor, D. E., 1971: A hyperbolic system for obtaining VHF radio pictures of lightning. *J. Geophys. Res.,* **76,** 1478–1489.

Rison, W. R., R. J. Thomas, P. R. Krehbiel, T. Hamlin, and J. Harlin, 1999: A GPS-based three-dimensional lightning mapping system: Initial observations in Central New Mexico. *Geophys. Res. Lett.,* **26,** 3573–3576.

Schultz, C. J., W. A. Petersen, and L. D. Carey, 2009: Preliminary development and evaluation of lightning jump algorithms for the real-time detection of severe weather. *J. Appl. Meteor. Climatol.,* in press.

Simmons, K. M., and D. Sutter, 2008: Tornado warnings, lead times, and tornado casualties: An empirical investigation. *Wea. Forecasting,* **23,** 246–258.

Steiger, S. M., R. E. Orville, and L. D. Carey, 2007: Total lightning signatures of thunderstorm intensity over north Texas. Part I: Supercells. *Mon. Wea. Rev.,* **135,** 3281–3302.

Stumpf, G. J., A. Witt, E. D. Mitchell, P. L. Spencer, J. T. Johnson, M. D. Eilts, K. W. Thomas, and D. W. Burgess, 1998: The National Severe Storms Laboratory mesocyclone detection algorithm for the WSR-88D. *Wea. Forecasting,* **13,** 304–326.

Thomas, R., P. Krehbiel, W. Rison, J. Hamlin, T. Harlin, and N. Campbell, 2003: The LMA flash algorithm. *Proc. 12th Int. Conf. on Atmospheric Electricity,* Veraille, France, International Commission on Atmospheric Electricity, ThC4-023-197.

Wiens, K. C., S. A. Rutledge, and S. A. Tessendorf, 2005: The 29 June 2000 supercell observed during STEPS. Part II: Lightning and charge structure. *J. Atmos. Sci.,* **62,** 4151–4177.

Wilks, D. S., 1995: *Statistical Methods in the Atmospheric Sciences*. Academic Press, 467 pp.

Williams, E. R., 2001: The electrification of severe storms. *Severe Local Storms, Meteor. Monogr.,* No. 50, Amer. Meteor. Soc., 527–561.

——, M. E. Weber, and R. E. Orville, 1989: The relationship between lightning type and convective state of thunderclouds. *J. Geophys. Res.,* **94,** 13 213–13 220.

——, and Coauthors, 1999: The behavior of total lightning activity in severe Florida thunderstorms. *Atmos. Res.,* **51,** 245–265.

Witt, A., M. D. Eilts, G. J. Stumpf, J. T. Johnson, E. D. Mitchell, and K. W. Thomas, 1998a: An enhanced hail detection algorithm for the WSR-88D. *Wea. Forecasting,* **13,** 286–303.

——, ——, ——, E. D. Mitchell, J. T. Johnson, and K. W. Thomas, 1998b: Evaluating the performance of WSR-88D severe storm detection algorithms. *Wea. Forecasting,* **13,** 513–518.